Soft Matter

PAPER

View Article Online
View Journal | View Issue

Cite this: *Soft Matter*, 2015, **11**, 5313

Rotational self-diffusion in suspensions of charged particles: simulations and revised Beenakker–Mazur and pairwise additivity methods†

Karol Makuch,*[a] Marco Heinen,[b] Gustavo Coelho Abade‡[c] and Gerhard Nägele[d]

Received 8th January 2015,
Accepted 23rd May 2015

DOI: 10.1039/c5sm00056d

www.rsc.org/softmatter

We present a comprehensive joint theory-simulation study of rotational self-diffusion in suspensions of charged particles whose interactions are modeled by the generic hard-sphere plus repulsive Yukawa (HSY) pair potential. Elaborate, high-precision simulation results for the short-time rotational self-diffusion coefficient, D^r, are discussed covering a broad range of fluid-phase state points in the HSY model phase diagram. The salient trends in the behavior of D^r as a function of reduced potential strength and range, and particle concentration, are systematically explored and physically explained. The simulation results are further used to assess the performance of two semi-analytic theoretical methods for calculating D^r. The first theoretical method is a revised version of the classical Beenakker–Mazur method (BM) adapted to rotational diffusion which includes a highly improved treatment of the salient many-particle hydrodynamic interactions. The second method is an easy-to-implement pairwise additivity (PA) method in which the hydrodynamic interactions are treated on a full two-body level with lubrication corrections included. The static pair correlation functions required as the only input to both theoretical methods are calculated using the accurate Rogers–Young integral equation scheme. While the revised BM method reproduces the general trends of the simulation results, it significantly underestimates D^r. In contrast, the PA method agrees well with the simulation results for D^r even for intermediately concentrated systems. A simple improvement of the PA method is presented which is applicable for large concentrations.

1 Introduction

Short-time translational diffusion properties of colloidal suspensions such as the translational self- and collective diffusion coefficients and the wavenumber-dependent hydrodynamic function, and short-time rheological properties including the high-frequency viscosity, have been the subject of numerous experimental studies.[1–7] These studies have been accompanied over the past few years by computer simulation (see, *e.g.* ref. 8 and 9) and theoretical studies.[10–19]

In addition to the diffusion properties associated with translational degrees of freedom of the particles, the colloidal short-time dynamics is characterized by transport coefficients related to rotational degrees of freedom. For monodisperse globular particles with spherically symmetric direct pair interaction, the respective key coefficient is the short-time rotational self-diffusion coefficient D^r. This coefficient depends on the internal hydrodynamic structure of the particles, and *via* the direct and solvent-mediated hydrodynamic interactions (HIs) also on the particle concentration and strength and the range of the effective pair potential.

Experimental studies of the short-time rotational self-diffusion coefficient, D^r, in concentrated suspensions of spherical particles are based on techniques which can distinguish different particle orientations. These methods include depolarized dynamic light scattering on optically anisotropic particles,[3] nuclear magnetic resonance,[20] time-resolved phosphorescence anisotropy[21–23] and polarized fluorescence recovery after photobleaching.[24] Most experimental work on rotational diffusion has been on monodisperse colloidal systems of neutral hard spheres and charge-stabilized particles, and here most notably on optically anisotropic fluorinated Teflon spheres,[3] and silica and polystyrene spheres labeled by a phosphorescent dye.[21–24] In addition, binary mixtures of charge-stabilized particles have been studied where

[a] *Faculty of Physics, Institute of Theoretical Physics, University of Warsaw, ul. Pasteura 5, 02-093 Warsaw, Poland. E-mail: Karol.Makuch@fuw.edu.pl*
[b] *Division of Chemistry and Chemical Engineering, California Institute of Technology, Pasadena, California 91125, USA*
[c] *Fachbereich Physik, Universität Konstanz, 78457 Konstanz, Germany*
[d] *Institute of Complex Systems (ICS-3), Research Centre Jülich GmbH, 52425 Jülich, Germany*

† Electronic supplementary information (ESI) available. See DOI: 10.1039/c5sm00056d

‡ On leave from: Departamento de Engenharia Mecânica, Universidade de Brasília, Campus Darcy Ribeiro, 70910-900, Asa Norte, Brasília-DF, Brazil.

one component is very dilute.[21–23] Since the particles are charged in most of the experimentally investigated suspensions, a systematic theoretical-simulation study of rotational self-diffusion in systems with electro-steric pair interactions is on demand.

A comprehensive analysis of the coefficient D^r in spherical-particle suspensions is of importance not only in its own right. The results of this analysis can serve as a reference for the study of the orientationally averaged rotational self-diffusion in dispersions of charge-stabilized particles with non-isotropic direct interactions and shapes such as Gibbsite platelets,[25] and with non-spherical surface hydrodynamic boundary conditions such as for patchy colloids (*e.g.*, Janus particles) and proteins (*e.g.*, lysozyme). The comparison with generic theoretical results for spherical particles allows us to investigate the significance of specific anisotropic interaction and surface boundary condition contributions. A practical application of a comprehensive analysis of D^r in charge-stabilized spherical-particle dispersions can be the micro-rheological estimate of the high-frequency viscosity based on the generalized Stokes–Einstein–Debye relation, if appropriately combined with the theoretical analysis of deviations from this approximate relation (see, *e.g.*, ref. 22 and 26).

While the short-time transport properties of spherical-particle dispersions are expressible theoretically as rather simple isotropic equilibrium averages invoking hydrodynamic mobility tensors, the difficulty in their actual calculation arises from the long-ranged many-body HIs between the particles. The slowing influence of the HIs is particularly pronounced when particles are in relative motion close to each other.

There exist two major theoretical solution schemes which have been used in the past for the calculation mainly of translational short-time diffusion properties and the high-frequency viscosity. The first one is the so-called pairwise additivity (PA) approximation. In its most complete version, all two-body HIs contributions are accounted for including lubrication terms, but three-body and higher order interaction contributions are disregarded. By construction, its application range is usually limited to semi-dilute systems, and in particular to charge-stabilized suspensions that are often hydrodynamically dilute even if the direct interactions are strong.[9] Regarding short-time self-diffusion coefficients and the high-frequency viscosity, however, the PA method can be profitably used also at higher concentrations, owing to the steep decay, with increasing inter-particle distances, of the hydrodynamic mobility tensors associated with these quantities.

Different from the PA scheme, the semi-analytical method of calculating short-time diffusion and viscosity properties by Beenakker–Mazur,[13–15] commonly referred to as the BM or $\delta\gamma$ method, is in principle applicable also to concentrated suspensions. To date, it has been considered to be the most comprehensive and versatile statistical physics approach to colloidal short-time dynamics. It is a mean-field-type approximation method which accounts for many-body HI contributions in the form of so-called ring self-correlation diagrams, without an account of lubrication effects. In its standard second-order version, the only required external input is the static structure factor, $S(q)$, as a function of scattering wavenumber q. A major short-coming of the original BM method is its poor treatment of the translational short-time self-diffusion coefficient D^t. This deficiency can be overcome by using a more accurate method for the self-part by using, *e.g.*, the PA approximation result for D^t for lower concentrated systems. The self-part corrected BM scheme has been applied both to suspensions of neutral and charge-stabilized particles,[7,9,26,27] for the calculation of the hydrodynamic and collective diffusion functions, and the high-frequency viscosity. It was applied recently also to suspensions of hydrodynamically structured particles,[28] and with certain additional approximations also to the cooperative diffusion in binary hard-sphere mixtures.[29] The predictions for these systems are decently good, with inaccuracies revealed at all concentrations. These inaccuracies can be partially attributed to the approximate treatment of the HIs in the original BM method, and partially to the invoked mean-field approximation. In recent work reported by Makuch and Cichocki,[30] the approximation steps in the original derivation of the BM method have been reduced, in particular by accounting for a large number of hydrodynamic multipoles in the truncated multipolar matrices which are extrapolated to infinite order. The observation that the revised BM method by Makuch and Cichocki, with its improved hydrodynamic mobility tensor treatment, has not resulted in a systematic improvement of the hydrodynamic function and high-frequency viscosity predictions points to a fortuitous cancellation of errors in the various approximation steps of the original method by Beenakker and Mazur.

Theoretical and simulation work on rotational self-diffusion has been done so far mainly for the two opposite limiting cases of dispersion of uncharged hard spheres, and low-salinity charge-stabilized suspensions, respectively, where the screening of the electrostatic interaction is weak. Very little is known about the broad transition region formed by dispersions with intermediate salinities.

Simulation work on rotational self-diffusion has dealt mainly with monodisperse systems of non-permeable[26,31,32] and permeable hard spheres.[33] Charge-stabilized systems have been addressed in few simulation studies only,[26,31] focussing on low-salinity systems.

The short-time rotational self-diffusion coefficient in hard-sphere suspensions was studied theoretically by various groups using truncated hydrodynamic cluster expansions up to quadratic order in the particle volume fraction ϕ.[3,34–36] The high-precision result by Cichocki *et al.*,[37]

$$\frac{D^r}{D_0^r} = 1 - 0.631\phi - 0.726\phi^2 + \mathcal{O}(\phi^3), \qquad (1)$$

includes a lubrication correction both for the two-body and three-body HI contributions. Here, $D_0^r = k_BT/(8\pi\eta a^3)$ is the single-particle rotational diffusion coefficient of a no-slip sphere of hydrodynamic radius a, and ϕ is the particle volume fraction. Quite interestingly, and as shown in ref. 26 and 33, the explicit quadratic form in eqn (1) describes simulation and experimental data remarkably well for volume fractions up to the hard-sphere freezing transition value $\phi_f = 0.494$, indicating that higher-order virial coefficients beyond the two- and three-body ones are small or mutually cancel out. Whether the good description of the (orientationally averaged) hard-sphere D^r by

two-body and three-body HIs contributions alone carries over to the high-concentration equilibrium crystal or metastable fluid phase regions is an open question remaining to be answered in a future simulation study.

The BM method has been applied to the rotational self-diffusion of uncharged hard spheres only, in a single paper by Treloar and Masters[38] where approximations along the line of those introduced by Beenakker and Mazur have been made. There has been so far no application of this method to rotational self-diffusion in charge-stabilized suspensions. The latter systems have been analyzed in the weak electrostatic screening regime using a simplified PA approximation approach based on a truncated inverse distance expansion of the two-body rotational mobility tensors, by considering in addition the leading-order long-distance hydrodynamic three-body term.[22,39,40] For charged particles with strong long-distance repulsion, the remarkable scaling relation,

$$\frac{D^{\mathrm{r}}}{D_0^{\mathrm{r}}} = 1 - a_{\mathrm{r}}\phi^2, \qquad (2)$$

with $a_{\mathrm{r}} \approx 1.3$ has been obtained by this simplifying approach. The comparison with Lattice-Boltzmann[31] and accelerated Stokesian dynamics simulation results[26] has shown that this relation applies accurately up to $\phi \approx 0.3$. Different from eqn (1) valid for neutral hard spheres, the scaling relation in eqn (2) is not a second-order virial expansion result. It originates basically from the $\phi^{-1/3}$ concentration scaling of the radius, r_{m}, of the nearest-neighbor shell of particles in low-salinity systems.[26]

The present article reports on the first comprehensive theoretical and simulation study of short-time rotational diffusion in suspensions of spherical particles whose static pair interactions are modeled by the hard-sphere plus repulsive Yukawa (HSY) pair potential. The generic HSY model has many applications ranging from classical charge-stabilized colloidal particle suspensions such as silica, fluorinated Teflon and polystyrene sphere systems to ionic microgels and globular protein solutions. We systematically explore a broad range of systems with fluid-like microstructure following two distinct paths in the universal HSY phase diagram. The rotational self-diffusion coefficient D^{r} along these two paths is calculated using three different methods, and salient trends in the behavior of D^{r} are identified and physically explained.

The first employed method is an elaborate hydrodynamic force multipole simulation method encoded in the HYDRO-MULTIPOLE program package.[37] Using this simulation tool, we have generated high-precision results for D^{r} in a broad range of volume fractions and pair potential strengths, for two largely different screening parameters characteristic of bcc and fcc type ordering tendencies, respectively, for systems near the universal fluid-solid freezing line. These simulation results have been obtained at the expense of a substantial numerical effort. They are used also as benchmarks for the accuracy assessment of the two additionally employed semi-analytic methods for calculating D^{r}.

The second method is a revised version of the original BM method for D^{r} by Treloar and Masters.[38] Different from their original method, in our newly derived revised BM method various approximation steps have been avoided. This includes in particular our highly improved treatment of the salient hydrodynamic interactions. The performance of the revised BM method is assessed by the comparison with the simulation results for D^{r}.

As the third method, we use a simplifying pairwise additivity (PA) method in which the rotational hydrodynamic mobility tensors are treated on the full two-body level including lubrication, without long-distance mobility tensor truncations being used as in earlier applications of the PA method to the HSY model. As we are going to show in comparison with our comprehensive simulation results, this semi-analytic and easy-to-implement method performs surprisingly well even up to intermediately large concentrations, with the trends of D^{r} being well reproduced. We further present an empirically motivated *ad hoc* improvement of the PA method applicable for concentrated suspensions.

Both the revised BM and the PA methods require the radial distribution function (RDF), $g(r)$, of the HSY model as the only input. The RDF and its associated static structure factor $S(q)$ are calculated using the Rogers–Young (RY) integral equation scheme known to be quite accurate for HSY systems. We discuss the shapes and general trends of the static pair functions to the extent required for the physical understanding of the general behavior of D^{r}.

The article is organized as follows: in Section 2, we give the essentials of short-time rotational self-diffusion. Section 3 includes the description of the HSY model with employed interaction parameters, and a discussion of the RY radial distribution functions used in the two semi-analytic methods of calculating D^{r}. The employed simulation method is briefly described in Section 4. The revised Beenakker–Mazur method and the PA method of calculating D^{r} are explained in Sections 5 and 6, respectively. Our results for the short-time rotational self-diffusion coefficient are presented and discussed in Section 7. The summary and final conclusions are contained in Section 8. Details of the derivation of the revised BM method, and of the hydrodynamic mobility matrices used in this method are given in part S1 and S2, respectively, of the ESI.†

2 Short-time rotational self-diffusion coefficient

We consider rotational diffusion in a fluid-state suspension of monodisperse spherical Brownian particles immersed in a structureless Newtonian solvent of shear viscosity η, on a coarse-grained Brownian time scale exceeding the rotational and translational momentum relaxation times $\tau_{\mathrm{B}}^{\mathrm{t}} \sim \tau_{\mathrm{B}}^{\mathrm{r}}$, respectively, by several orders of magnitude.[3,41] On this scale, particles and fluid move quasi-inertia-free, and the solvent-mediated HIs act quasi-instantaneously. The configurational evolution of the particles is then governed by the generalized Smoluchowski equation[42–44] for the N-particle probability density function $p(\mathbf{R}_1,\ldots,\mathbf{R}_N,\hat{\mathbf{u}}_1,\ldots,\hat{\mathbf{u}}_N,t)$ of the sphere center positions $\mathbf{R}_1,\ldots,\mathbf{R}_N$ and orientations $\hat{\mathbf{u}}_1,\ldots,\hat{\mathbf{u}}_N$ at time t. The associated low-Reynolds-number incompressible fluid

flow is described by the linear stationary Stokes equation.[45] The hydrodynamic ingredients to the generalized Smoluchowski equation derived from the Stokes equation are the translational–rotational mobility tensors quantifying the linear relations,

$$\mathbf{U}_i = \sum_{j=1}^{N} \boldsymbol{\mu}_{ij}^{\mathrm{tt}}(\mathbf{R}_1 \ldots \mathbf{R}_N) \cdot \mathbf{F}_j + \sum_{j=1}^{N} \boldsymbol{\mu}_{ij}^{\mathrm{tr}}(\mathbf{R}_1 \ldots \mathbf{R}_N) \cdot \mathbf{T}_j, \qquad (3)$$

$$\boldsymbol{\Omega}_i = \sum_{j=1}^{N} \boldsymbol{\mu}_{ij}^{\mathrm{rt}}(\mathbf{R}_1 \ldots \mathbf{R}_N) \cdot \mathbf{F}_j + \sum_{j=1}^{N} \boldsymbol{\mu}_{ij}^{\mathrm{rr}}(\mathbf{R}_1 \ldots \mathbf{R}_N) \cdot \mathbf{T}_j, \qquad (4)$$

between the forces and torques, $\mathbf{F}_j$ and $\mathbf{T}_j$, respectively, acting on the colloidal spheres, and the resulting translational and rotational particle velocities $\mathbf{U}_i$ and $\boldsymbol{\Omega}_i$. For the uniformly assumed no-slip hydrodynamic surface boundary condition, the mobility tensors are independent of the particle orientations.

In depolarized dynamic light scattering,[3,46] the short-time rotational self-diffusion coefficient of Brownian spheres is determined from the initial decay of the measurable orientational self-correlation function, for correlation times t within $\tau_B^r \ll t \ll 1/D_0^r$ where particle orientations and positions have changed by very small amounts only, on the characteristic length scale of the suspension. For a concentrated isotropic suspension, D^r can be computed as the ensemble average of the trace of the rotational mobility tensor expression,[47]

$$D^r = \frac{k_B T}{3} \lim_{\infty} \left[\mathrm{Tr} \left\langle \frac{1}{N} \sum_{i=1}^{N} \boldsymbol{\mu}_{ii}^{\mathrm{rr}}(\mathbf{R}_1 \ldots \mathbf{R}_N) \right\rangle \right]. \qquad (5)$$

where $\langle \cdots \rangle$ is an equilibrium ensemble average, and where the thermodynamic limit $N \to \infty$ at fixed particle concentration has been taken. It should be noted that D^r as given in eqn (5) is, for non-zero concentrations, different from the initial slope of the mean-squared displacement of the particle orientation unit vector $\hat{\mathbf{u}}_i(t)$.

3 Static correlations of HSY particles

The pair potential in the hard-sphere plus repulsive Yukawa (HSY) model is given by

$$\frac{u(r)}{k_B T} = \begin{cases} \gamma \dfrac{\exp\{-\kappa(r-\sigma)\}}{r/\sigma}, & r > \sigma \\ \infty, & r < \sigma \end{cases}, \qquad (6)$$

where $\gamma \geq 0$ is the coupling parameter of the Yukawa-type potential part, $\sigma = 2a$ the hard-core diameter, r the center-to-center distance between two spheres, k_B the Boltzmann constant, and T the absolute temperature. The range of the HSY potential is set by the inverse of the screening parameter $\kappa \geq 0$. In the infinite screening limit $\kappa \to \infty$, or likewise for $\gamma = 0$, the hard-sphere potential is recovered. In the opposite limit $\kappa \to 0$ of zero-screening, a one-component plasma-like system is described.

Dispersions which can be described by the HSY model range from charge-stabilized suspensions of rigid colloidal spheres[48] to globular protein solutions[49] and dusty plasmas.[50] The HSY potential form is in general a good approximation to the state-dependent effective pair-potential between charged colloidal spheres. The latter is obtained from integrating out the degrees of freedom of the microions and solvent molecules. In many experimentally encountered suspensions, the short-ranged van der Waals attraction neglected in the HSY model is of no relevance, either since the electrostatic repulsion between the particles is strong enough to prevent near-contact configurations,[7] or the solvent dielectric constant nearly matches that of the suspended particles,[51–54] or the particles are sterically stabilized by grafted polymers.[55] The complicated dependencies of the state-dependent potential parameters γ and κ in charge-stabilized suspensions on the salt ion concentration, colloidal volume fraction, and bare and effective colloidal surface charges are the topic of on-going research that covers experiments, theory and computer simulations.[56–67] The present work is not concerned with a first-principles determination of the state-dependence and here in particular the concentration dependence of γ and κ, with the two reduced interaction parameters influenced also by the specific electrochemistry at the surfaces of the dispersed particles. Instead, γ and κ are treated quite generally as individually variable parameters. Note further that the direct interactions in the HSY model are treated as pairwise additive. Non-pairwise additivity effects in the direct interaction of charged colloidal particles are usually quite small.[68]

According to eqn (6), the thermodynamic state of the HSY model, and likewise the RDF as a function of r/σ, are fully characterized by three independent non-dimensional parameters which can be taken as $\kappa\sigma$, γ and the particle volume fraction

$$\phi = \pi\sigma^3 n/6, \qquad (7)$$

where n is the number density of particles. For truly charge-stabilized suspensions, however, the physical hard-core is masked by the strong Yukawa repulsion, *i.e.* the likelihood for two or more spheres being in contact is negligibly small. The appropriate physical length scale for these so-called point-Yukawa systems is the geometric mean particle distance $\langle r \rangle = n^{-1/3}$, and the thermodynamic state and in particular the phase boundaries are determined by two parameters only. The phase boundaries of the point-Yukawa system look particularly simple, with nearly straight lines, in the two-dimensional $(\lambda, \tilde{T})$ phase diagram representation[69,70] where

$$\lambda = \kappa \langle r \rangle, \qquad (8)$$

$$\tilde{T} = \frac{k_B T}{u(\langle r \rangle)}, \qquad (9)$$

are the reduced screening parameter and the inverse reduced Yukawa interaction parameter, respectively. In terms of these parameters, the dominating Yukawa-part of the HSY potential reads

$$\frac{u(x)}{k_B T} = \frac{\exp\{-\lambda(x-1)\}}{\tilde{T} x}, \qquad (10)$$

where $x = r/\langle r \rangle$ with $x > \sigma/\langle r \rangle$. If considered as a function of x and $q\langle r \rangle$, the RDF $g(r)$ and static structure factor $S(q)$ of point-Yukawa particles are uniquely determined by the state point $(\lambda, \tilde{T})$.

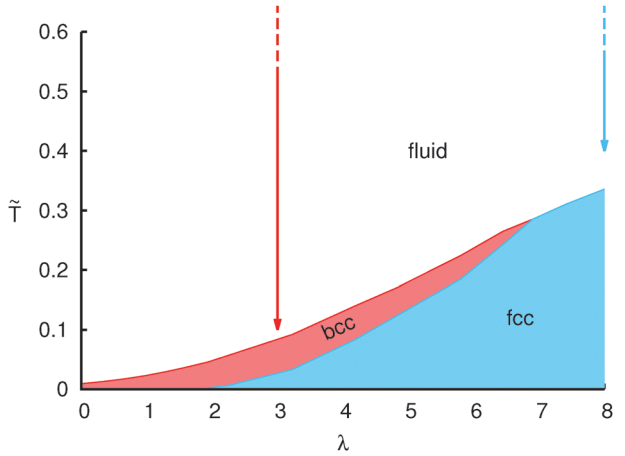

Fig. 1 Schematic (λ, $\tilde{T}$) phase diagram of the hard-core plus repulsive Yukawa (HSY) system with masked hard-core interactions (point-Yukawa system). The arrows indicate the two fluid-state pathways towards the fluid-bcc and fluid-fcc phase boundary lines, respectively, followed in our calculations of the short-time rotational self-diffusion coefficient. The left arrow corresponds to λ = 3 and $\tilde{T}$ = 0.1, 0.2, 0.5, 1, 2, 5, 10, 20, 50, 100, 200, 500, 1000, and the right one to λ = 8 and $\tilde{T}$ = 0.4, 0.6, 0.8, 1, 2, 5, 10, 20, 50, 100, 200, 500, 1000. The volume fractions considered in both pathways are ϕ = 0.05, 0.15, 0.25, 0.35.

A sketch of the (λ, $\tilde{T}$) phase diagram of point-Yukawa particles is given in Fig. 1. It consists of a high-temperature supercritical fluid phase, separated by a fluid-solid coexistence boundary from a face-centered-cubic (fcc) solid phase region at high screening, and a body-centered-cubic (bcc) solid phase region at low screening. There is a single triple point of three-phase coexistence at $\lambda_t \approx 6.9$.[69,71] According to ref. 72 and 73 the fluid-solid coexistence boundary determined in simulations is well reproduced by the RY integral equation scheme in conjunction with the Hansen–Verlet criterion $S(q_m) = 3.1$ for the onset of freezing, where q_m is the wavenumber position of the static structure factor maximum.

The full phase diagram of the HSY model including systems with significantly non-zero RDF contact values $g(r = \sigma^+) > 0$ is more complicated, and requires the specification of a third reduced parameter in addition to, say, λ and $\tilde{T}$, namely the volume fraction ϕ. As shown in simulations by Hynninen and Dijkstra,[71] there is then an additional triple point at very small λ associated with large volume fractions where the fcc phase is favored. Provided the coupling parameter in eqn (6) is sufficiently large (*i.e.* $\gamma \geq 20$) and ϕ sufficiently small (*i.e.* $\phi < 0.5$), the phase coexistence lines of the HSY model can be essentially mapped to those of the point-Yukawa model, by expressing γ and $\kappa\sigma$ in eqn (6) in terms of $\{\lambda, \tilde{T}, \phi\}$ using $\langle r \rangle \propto \phi^{-1/3}$. Note that for $\tilde{T} > 1$, the potential energy of the Yukawa potential part at mean particle distance is smaller than the thermal energy k_BT. With increasing $\tilde{T}$ and fixed λ and ϕ, the importance of the Yukawa potential part diminishes, and the suspension becomes increasingly hard-sphere like.

The present study of short-time rotational diffusion is restricted to the fluid phase regime. However, it is interesting to compare changes in rotational diffusion when the fluid-bcc and fluid-fcc parts of the fluid-solid coexistence lines are approached, respectively, upon decreasing the reduced inverse Yukawa interaction parameter $\tilde{T}$. To this end, in our simulation and theoretical calculations of D^r we follow two distinct pathways indicated by the two arrows in the (λ, $\tilde{T}$) diagram in Fig. 1. The left pathway is the vertical line along λ = 3 with the reduced inverse Yukawa interaction parameter series $\tilde{T} \in \{0.1, 0.2, 0.5, 1, 2, 5, 10, 20, 50, 100, 200, 500, 1000\}$, where the smallest value $\tilde{T}$ = 0.1 describes a state point close to the fluid-bcc phase boundary line part of the point-Yukawa phase diagram. The right pathway in the figure is the line along λ = 8 with values $\tilde{T} \in \{0.4, 0.6, 0.8, 1, 2, 5, 10, 20, 50, 100, 200, 500, 1000\}$. Here, the lowest value $\tilde{T}$ = 0.4 is close to the fluid-fcc phase boundary line part. For both pathways, the volume fraction is selected as ϕ = 0.05, 0.15, 0.25 and 0.35, respectively. This amounts to simulation-based calculations of D^r at 104 different fluid-phase state points. The static structure factors $S(q)$ and the associated RDFs $g(r)$ of all HSY systems explored in the present work have been calculated using the RY integral equation scheme described in the following subsection. We have checked that each of the considered $S(q)$'s qualifies as a liquid-state structure factor according to the empirical Hansen–Verlet criterion. This criterion states that at freezing into a solid phase, $S(q_m)$ attains a value near 3.1 for point-Yukawa systems. For HSY systems with RDF contact values $g(\sigma^+)$ significantly larger than zero, the values of $S(q_m)$ at freezing vary in between 3.1 and 2.85, with the lower value attained by a pure hard-sphere system.[70,74–76]

3.1 Rogers–Young scheme

The revised $\delta\gamma$ method and the PA scheme require $g(r)$ as the only input. We obtain $g(r)$ numerically by solving the Ornstein–Zernike equation,[77]

$$h(r) = c(r) + n\int d^3r' c(r') h(|\mathbf{r} - \mathbf{r}'|) \qquad (11)$$

for a three-dimensional, homogeneous and isotropic fluid in conjunction with the approximate RY[78] closure relation invoking the HSY pair potential,

$$\frac{u(r)}{k_BT} + \ln g(r) = \ln\left[1 + \frac{\exp\{[h(r) - c(r)]f(r)\} - 1}{f(r)}\right]. \qquad (12)$$

Here, $h(r) = g(r) - 1$ is the total correlation function, $c(r)$ is the direct correlation function, and n is the particle number density. Eqn (12) includes the mixing function $f(r) = 1 - \exp\{-\alpha r\}$ with the non-negative inverse length parameter α. This parameter is determined self-consistently by requiring equality of the isothermal osmotic compressibilities derived from the compressibility equation,

$$\left(\frac{\partial P_c/(k_BT)}{\partial n}\right)_T = 1 - 4\pi n\int_0^\infty dr r^2 c(r) \qquad (13)$$

and the numerically differentiated virial pressure equation,

$$\frac{P_v}{nk_BT} = 1 + \frac{2\pi}{3}n\left\{\sigma^3 g(\sigma^+) - \frac{1}{k_BT}\int_0^\infty dr r^3 g(r)\frac{du(r)}{dr}\right\}, \qquad (14)$$

where P_c and P_v are the isothermal osmotic pressure in the compressibility and virial equation, respectively.

In using eqn (14), we neglect any thermodynamic state dependence of the pair potential. As noted further up this section already, a consequence of integrating out the microionic and solvent degrees of freedom is that the resulting effective pair potential of the HSY form is in general dependent on the particle concentration n and the system temperature T (see, *e.g.*, ref. 67). This gives rise to additional terms on the right-hand-side of eqn (14) invoking the partial derivative of $u(r)$ with respect to n and T. The precise form of the effective pair potential depends on the specific electro-chemical surface properties of the colloidal spheres, and the specific properties of the suspending electrolyte solution. Since we are not dealing here with the microscopic theory of effective colloidal pair potentials but with the generic behavior of D^r, in taking the concentration derivative of P_v in eqn (14) we disregard any specific state dependence of $u(r)$, and of the RY mixing parameter α.

Our numerical solution of the RY integral equation for broad ranges of volume fractions, screening and interaction parameters has been facilitated by using a spectral solver described in ref. 66. The good accuracy of the RY approximation for HSY systems was demonstrated in various studies[26,41,53,54,79,80] comprising comparisons with simulation and experimental data.

3.2 Radial distribution function in the RY scheme

Owing to the rather steep $\mathcal{O}(1/r^6)$ long-distance decay of the rotational mobility tensor $\boldsymbol{\mu}_{ii}^{rr}$ associated with D^r (see Section 6), the rotational diffusion coefficient is quite sensitive to the shape of the RDF at small particle separations. This motivates the following discussion on the behavior of $g(r)$ in the (λ, $\tilde{T}$, ϕ) fluid-phase parameter regime of the HSY model explored in this work.

In Fig. 2, the RY calculated RDFs (upper panel) and structure factors (lower panel) for ϕ = 0.25 and λ = 8 are depicted for different inverse Yukawa interaction parameters $\tilde{T}$ as indicated in the figure. The strength of the Yukawa potential at the mean particle distance, in units of the thermal energy, decreases with increasing $\tilde{T}$. For the largest considered value $\tilde{T}$ = 1000, the HSY system at ϕ = 0.25 reduces essentially to a hard-sphere fluid, with the RDF maximum $g(r_m)$ located at contact distance $r_m = \sigma$. With decreasing $\tilde{T}$, the increasingly strong Yukawa repulsion reduces the relative probability, $g(\sigma^+)$, of two-sphere contact, and it also lowers the compressibility factor $S(0)$. Moreover, the nearest neighbor shell of spheres around the radial distance r_m where $g(r)$ has its maximum moves outwards and sharpens with decreasing $\tilde{T}$. For the lowest considered value $\tilde{T}$ = 0.4 corresponding to a fluid state point near the fluid-fcc phase boundary line, the hard core of the particles is masked and $r_m \approx \langle r \rangle$.

A measure of the importance of the hard-core part of $u(r)$ relative to the Yukawa part is given by the RDF contact value $g(\sigma^+)$ plotted in Fig. 3 for all considered fluid-phase points (λ, $\tilde{T}$, ϕ). With increasing $\tilde{T}$, the relative strength of the Yukawa potential part ceases, and a plateau region of the RDF contact value is approached, characteristic of hard-sphere-like behavior. This is obviated by the horizontal line segments shown at the right

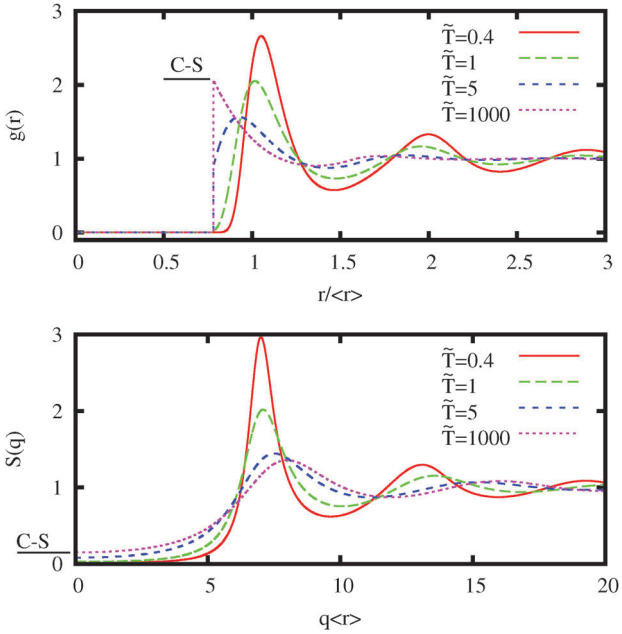

Fig. 2 Upper panel: RDF, $g(r)$, predicted by the Rogers–Young scheme for a HSY fluid system with λ = 8 and ϕ = 0.25. Four inverse Yukawa interaction parameters $\tilde{T}$ = 0.4, 1, 5, 1000 are considered as indicated. The horizontal line segment marks the Carnahan–Starling (C–S) contact value of hard spheres given by eqn (15). Lower panel: static structure factor, $S(q)$, corresponding to the displayed radial distribution functions in the upper panel. Horizontal line segment: C–S compressibility factor of hard spheres according to eqn (16). Pair distance r and wavenumber q are scaled with the geometric mean particle distance $\langle r \rangle$.

ordinate of the figure which mark the Carnahan–Starling (C–S) RDF contact values of hard spheres with vanishing Yukawa tail repulsion (γ = 0), given by

$$g_{HS}^{CS}(\sigma^+) = \frac{1 - \frac{1}{2}\phi}{(1-\phi)^3}. \quad (15)$$

We quote in addition the C–S equation,

$$S_{HS}^{CS}(q=0) = \frac{(1-\phi)^4}{(1+2\phi)^2 + \phi^3(\phi-4)}, \quad (16)$$

for the compressibility factor of hard spheres. The origin of the excellent accuracy of the semi-phenomenological C–S expressions for hard spheres is still a riddle, and a topic of ongoing research.[81] We emphasize that the employed RY scheme is a quite accurate but nevertheless approximate integral equation scheme. Its partial thermodynamic self consistency does not imply, *e.g.*, perfect agreement of the RY contact value for hard spheres with the practically exact Carnahan–Starling result in eqn (15). In fact, the RY scheme is lacking thermodynamic self-consistency with respect to any thermodynamic property except for the pressure. An extended version of the RY scheme (named ERY scheme) has been introduced by Carbajal-Tinoco,[82] which further improves the accuracy of the original RY scheme by introducing a second mixing parameter. In this more elaborate scheme, which however is not applicable to pure hard spheres

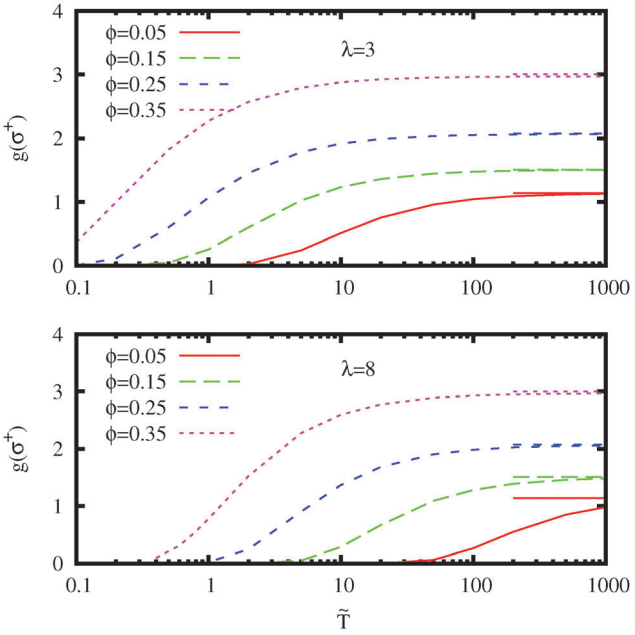

Fig. 3 Contact value, $g(\sigma^+)$, of the HSY-RY $g(r)$ as a function of $\tilde{T}$, for volume fractions ϕ = 0.05, 0.15, 0.25, 0.35 as indicated. Upper panel: λ = 3. Lower panel: λ = 8. Horizontal line segments for large $\tilde{T}$ mark the C–S hard-sphere contact values according to eqn (15).

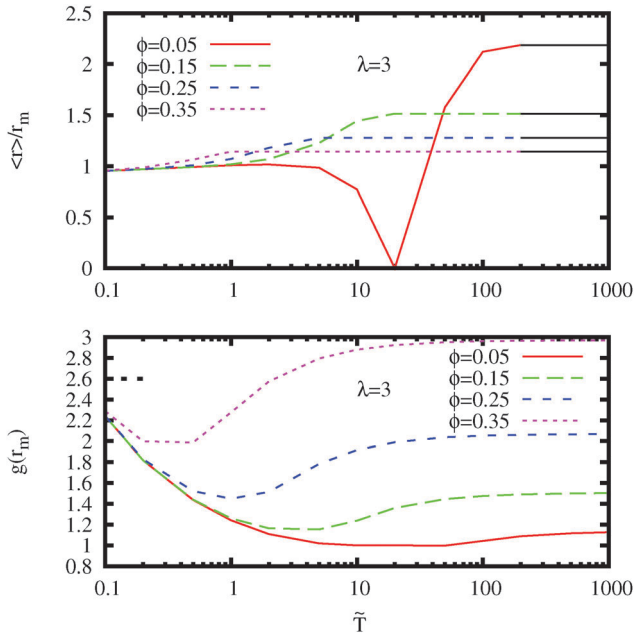

Fig. 4 Upper panel: inverse reduced position, $\langle r\rangle/r_m$, of the principal peak of $g(r)$ as a function of $\tilde{T}$, for λ = 3 and values of ϕ as indicated. The horizontal solid line segments at large $\tilde{T}$ indicate the inverse reduced contact distance, $\langle r\rangle/\sigma$, for the respective ϕ values. Lower panel: principal peak value, $g(r_m)$, of the RDF for the same set of parameters. The dashed horizontal line segment at small $\tilde{T}$ indicates the one-component plasma isochoric freezing transition value attained in the zero-screening limit $\lambda \to 0$ (see ref. 73).

without soft repulsion, the two mixing parameters are determined by enforcing thermodynamic self-consistency both regarding the pressure and the excess internal energy per particle. For the sake of simplicity and numerical stability, we have refrained from using the ERY scheme in the present work.

On first sight, it is surprising that in accordance with Fig. 3, the likelihood of observing two closely spaced particles is larger for λ = 3 than for λ = 8, for equal ϕ and $\tilde{T}$, even though the screening length of the Yukawa tail is significantly shorter in the latter case. This can be understood as follows: while the potential value $\beta u(x=1) = 1/\tilde{T}$ at $r = \langle r\rangle$ is equal for both λ values, the repulsive force, $-\beta\, \mathrm{d}u/\mathrm{d}x(x=1) = (1+\lambda)/\tilde{T}$, is larger in the λ = 8 case. Taken together with the substantially steeper rise of the Yukawa potential with decreasing x for λ = 8, this explains the lower probability of finding two closely spaced particles. For fixed λ, the small-$\tilde{T}$ region where the hard core is masked (*i.e.* where $g(\sigma^+) \approx 0$) shrinks with increasing ϕ, as it is expected.

For the upcoming discussion of D^r, it is relevant to investigate how the principal RDF maximum $g(r_m)$, and its position r_m, depend on the pair potential parameters. We notice first from Fig. 2 that r_m equals the smallest radial distance $r \geq \sigma$ where the derivative of $g(r)$ turns negative.

The dependence of $g(r_m)$ and r_m on $\tilde{T}$ is shown in Fig. 4 for λ = 3, and in Fig. 5 for λ = 8. According to both figures, for fixed ϕ and therefore fixed mean particle distance $\langle r\rangle$, the inverse principal peak location, $\langle r\rangle/r_m$, increases with decreasing Yukawa potential strength, *i.e.* increasing $\tilde{T}$, towards the limiting inverse reduced contact distance, $\langle r\rangle/\sigma$, of neutral hard spheres. The limiting hard-sphere values for the considered ϕ values are indicated by the horizontal solid line segments at the large-$\tilde{T}$ end of the upper panels in Fig. 4 and 5. Except for λ = 8 and the lowest considered volume fraction ϕ = 0.05, the hard-sphere limiting values have been all reached for $\tilde{T}$ = 1000. It is for this latter (λ, ϕ) point where the minimum of $g(r_m)$ as a function of $\tilde{T}$

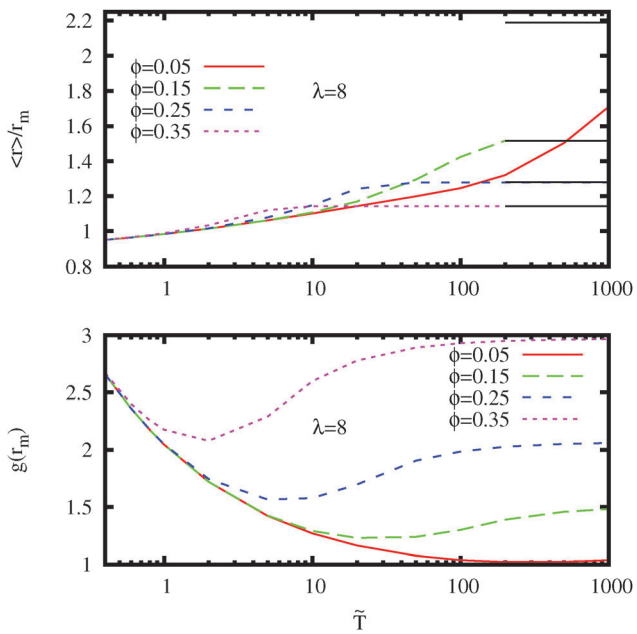

Fig. 5 Upper and lower panels: the same as in the upper and lower panel of Fig. 4, respectively, but for λ = 8.

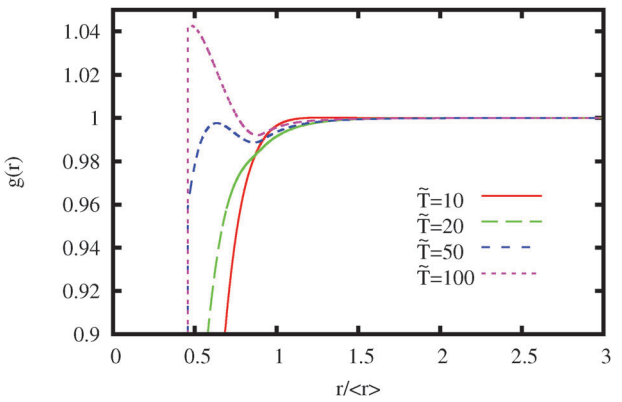

Fig. 6 HSY-RY $g(r)$ for $\phi = 0.05$ and $\lambda = 3$. Employed values of $\tilde{T}$ are $\tilde{T} = 10, 20, 50, 100$ as indicated.

observed in all depicted curves in the lower panels of Fig. 4 and 5 has its largest $\tilde{T}$ value. The minimum in $g(r_m)$ originates from the competition of Yukawa repulsion and excluded volume interaction (see here again Fig. 2 for $g(r)$). This competition is enforced with increasing concentration, reflected by a more pronounced minimum moving inwards to smaller values of $\tilde{T}$.

Note that the only exception from the monotonic behavior of r_m as a function of $\tilde{T}$ is the curve in the upper panel of Fig. 4 for $\lambda = 3$ and $\phi = 0.05$. To explain the peculiar shape of this curve, in Fig. 6 we plot associated RDFs, for values of $\tilde{T}$ as indicated. For large $\tilde{T} \geq 50$, the principal maximum of $g(r)$ is located close to $r = \sigma$. The maximum decreases and is shifted to larger distances r_m with decreasing $\tilde{T}$. At $\tilde{T} = 20$, no localized principal maximum is present any more, and $g(r)$ monotonically increases with increasing r so that $r_m = \infty$. When $\tilde{T}$ is further decreased, the strengthened Yukawa repulsion causes the reappearance of a RDF maximum at a distance r_m significantly larger than σ which is decreasing towards $\langle r \rangle$.

4 Simulation method

We have calculated D^r for no-slip spheres to high precision using a hydrodynamic multipole method corrected for lubrication,[37,83–85] and encoded in the HYDROMULTIPOLE program package.[37] The values for D^r have been determined from equilibrium configuration averages using typically $N = 256$ spheres interacting with the HSY potential, and placed in a periodically replicated cubic simulation box. At least 150 independent and fully equilibrated configurations for each parameter set $(\lambda, \tilde{T}, \phi)$ were used in calculating D^r based on eqn (5), generated by canonical ensemble Monte Carlo simulations. This has resulted in a low statistical relative error of less than 0.001. As reported in ref. 33, the calculated values for $D^r(N)$ using the periodic simulation box with N particles are not critically dependent on the system size. Therefore, no system size correction extrapolating to an infinitely large system is required as for short-time collective diffusion properties. Our elaborate simulation study for the two pathways in the HSY model phase diagram depicted in Fig. 1 covers in total 104 different fluid-phase state systems.

5 Revised Beenakker–Mazur method

In addition to our simulation analysis, we have calculated D^r using the revised Beenakker–Mazur (BM) method. Our revised version of this statistical physics approach, which has been extended by Treloar and Masters to the short-time rotational diffusion of hard spheres,[38] differs from the original one in that various approximation steps made originally have been avoided. This concerns in particular our severely improved treatment of the salient hydrodynamic interactions which in the original BM and Treloar and Masters method were described quite approximately. For details of how the rotational and translational hydrodynamic mobility tensors appearing in eqn (4) and (3) are calculated in the revised BM method, we refer to part S2 of the ESI.† Like in reported numerical applications of the original BM method, in the revised method we employ a renormalized concentration fluctuation expansion truncated to second order so that two-body static correlation functions are needed as the only static input. Different from the original BM method in which $S(q)$ constitutes this input, the RDF $g(r)$ is required as a direct input in the revised method.

A detailed discussion of the revised BM method for short-time rotational and translational self-diffusion with focus on the physical picture underlying the employed renormalized fluctuation expansion is given in part S1 of the ESI.†

6 Pairwise additivity approximation

The rotational hydrodynamic mobility tensor $\boldsymbol{\mu}_{ii}^{rr}(\mathbf{R}_1 \ldots \mathbf{R}_N)$ of N spherical particles in an infinite, quiescent fluid linearly relates the hydrodynamic torque $\mathbf{T}_i$ acting on a particle i to its rotational velocity $\boldsymbol{\Omega}_i$. By disregarding three-body and higher order hydrodynamic cluster contributions, one can approximate the exact N-particle rotational hydrodynamic mobility tensor by a sum of two-particle contributions,

$$\boldsymbol{\mu}_{ii}^{rr}(\mathbf{R}_1 \ldots \mathbf{R}_N) \approx \mu_0^r \left[1 + \sum_{n=1; n \neq i}^{N} \omega_{11}^{rr}(\mathbf{R}_i - \mathbf{R}_n) \right], \qquad (17)$$

where $\mu_0^r = D_0^r / k_B T$ is the single-sphere rotational mobility coefficient and 1 the three-dimensional unit tensor. The two-sphere tensor $\omega_{11}^{rr}(\mathbf{R}_i - \mathbf{R}_n)$ describes the hydrodynamic self-interaction of sphere i by means of flow reflections at a second sphere labeled by n, in the absence of the $N - 2$ other particles. This constitutes the pairwise additivity (PA) approximation where it is assumed that the HIs between two spheres are not disturbed by other ones. In principle, this assumption is justified for semi-dilute systems only.

Upon exploiting the axial symmetry of the two-sphere problem, the two-sphere tensor can be split into longitudinal and transversal components,

$$\omega_{11}^{rr}(\mathbf{R}_i - \mathbf{R}_n) = \alpha_{11}^{rr}(R_{in}) \hat{\mathbf{R}}_{in} \hat{\mathbf{R}}_{in} + \beta_{11}^{rr}(R_{in})[1 - \hat{\mathbf{R}}_{in} \hat{\mathbf{R}}_{in}], \qquad (18)$$

with $\hat{\mathbf{R}}_{in} = (\mathbf{R}_i - \mathbf{R}_n)/R_{in}$ and $R_{in} = |\mathbf{R}_i - \mathbf{R}_n|$.

In terms of the scalar longitudinal and transversal functions $\alpha_{11}^{rr}(R)$ and $\beta_{11}^{rr}(R)$, the normalized short-time rotational

self-diffusion coefficient is expressed in PA approximation by[3,39,40]

$$\frac{D^{r}}{D_0^{r}} = 1 + 8\phi\int_1^\infty \mathrm{d}x\, x^2 g(x)\left[\alpha_{11}^{rr}(x) + 2\beta_{11}^{rr}(x)\right], \qquad (19)$$

where $x = r/\sigma$ is here the two-sphere center-to-center distance in units of the sphere diameter $\sigma = 2a$. The functions $\alpha_{11}^{rr}(r)$ and $\beta_{11}^{rr}(r)$ can be calculated recursively in the form of a power series in the reduced inverse pair distance a/r. For the no-slip hydrodynamic surface boundary condition employed in this work, the leading-order (far-field) contributions are

$$\alpha_{11}^{rr}(r) = -3\left(\frac{a}{r}\right)^8 + \mathcal{O}\left(\left(\frac{a}{r}\right)^{10}\right), \qquad (20)$$

$$\beta_{11}^{rr}(r) = -\frac{15}{4}\left(\frac{a}{r}\right)^6 - \frac{39}{4}\left(\frac{a}{r}\right)^8 + \mathcal{O}\left(\left(\frac{a}{r}\right)^{10}\right), \qquad (21)$$

with higher-order terms in the expansion given in ref. 45 and 86. At near-contact distance $r \approx 2a$ where lubrication comes into play, the expansions in eqn (20) and (21) converge only slowly. In our numerical implementation of the PA method, we therefore use high-order series expansion results obtained by Jeffrey and Onishi.[87] On using the zero concentration hard-sphere RDF, $g(x) = \Theta(x - 1)$, in eqn (19), where $\Theta(x)$ is the unit step function, we have numerically checked that our code precisely reproduces the first-order virial coefficient value -0.631 in eqn (1). This demonstrates the high accuracy of the employed tabulated values for $\alpha_{11}^{rr}(r)$ and $\beta_{11}^{rr}(r)$ also at near-contact distances.

To our knowledge, the present PA method of calculating D^r is the first one where two-sphere hydrodynamic interactions have been fully accounted for general HSY systems, and not only for the limiting case of uncharged hard spheres. In earlier PA calculations of D^r for HSY systems with masked excluded volume interactions, only approximate far-field hydrodynamic mobility tensor expressions have been used. The PA method can be straightforwardly implemented. As it is noticed from eqn (19), a one-dimensional numerical integration is required only, with $g(r)$ as the static input.

7 Results and discussion

Our simulation and theoretical results for D^r/D_0^r as a function of inverse reduced Yukawa interaction parameter $\tilde{T}$ are depicted in Fig. 7–10, for volume fractions $\phi = 0.05$–0.35. In each figure, the results for the vertical fluid-phase pathway at $\lambda = 3$ directed towards the fluid-bcc phase coexistence line are compared with the results for the pathway at $\lambda = 8$ directed towards the fluid-fcc coexistence line (*cf.* Fig. 1). Note the different ordinate scales in the four figures, selected to highlight the differences in the theoretical and simulation results for D^r.

We start with discussing our high-precision simulation results for the considered HSY systems. The slowing influence of the HIs on rotational self-diffusion increases when the likelihood for small-distance particle pairs increases. According to our discussion of the RDFs in Fig. 3, the particles for $\lambda = 8$ repel each other more strongly than those for $\lambda = 3$, so that the radial region where $g(r)$ is small is more extended in the former case. This explains why all curves of D^r for $\lambda = 8$ are located above those for $\lambda = 3$, for all considered volume fractions. The HSY

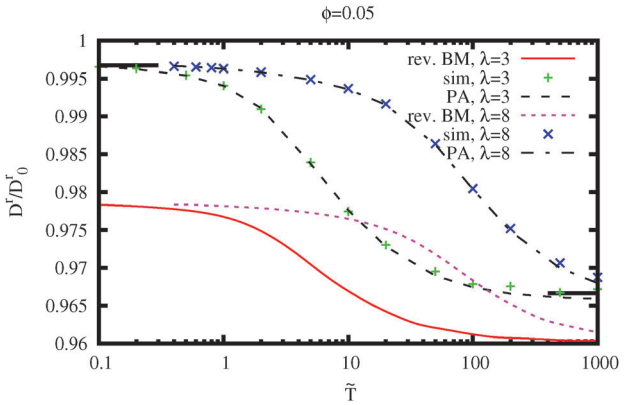

Fig. 7 Normalized rotational self-diffusion coefficient, D^r/D_0^r, as a function of $\tilde{T}$, for $\lambda = 3$ and 8, and $\phi = 0.05$. Simulation data (plus symbols and crosses) are compared with revised BM method predictions (solid and short-dashed curves) and PA method predictions (dashed-dotted and long-dashed curves). The theory and simulation values of D^r for $\lambda = 8$ are in general larger than the respective ones for $\lambda = 3$. Horizontal solid segment at large $\tilde{T}$: hard-sphere value according to eqn (1). Horizontal solid line segment at small $\tilde{T}$: scaling prediction in eqn (2) for low-salinity charge-stabilized systems.

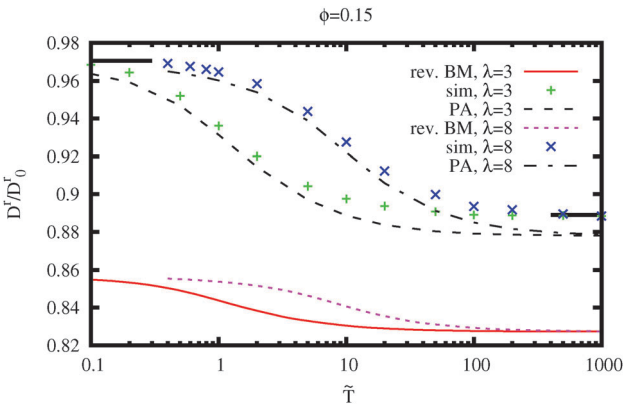

Fig. 8 Same as in Fig. 7 but for $\phi = 0.15$.

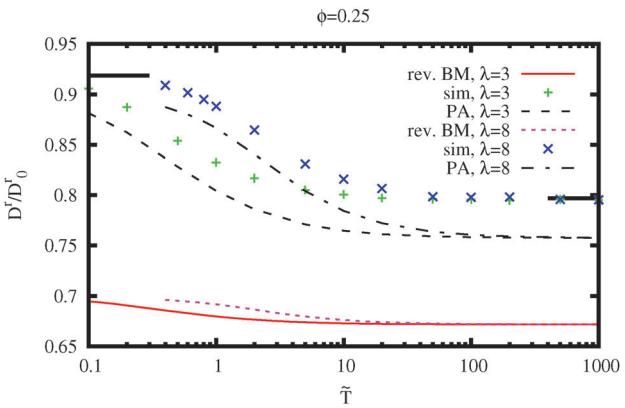

Fig. 9 Same as in Fig. 7 but for $\phi = 0.25$.

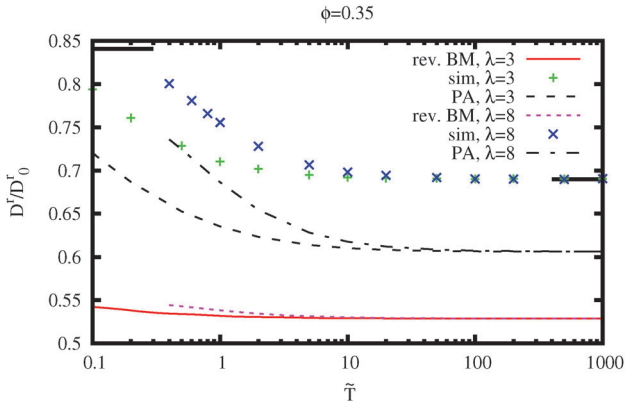

Fig. 10 Same as in Fig. 7 but for ϕ = 0.35.

particles can approach each other more closely with increasing $\tilde{T}$. This is reflected in curves for D^r which are monotonically decreasing.

As discussed earlier, at large values of $\tilde{T}$ a plateau region of D^r is reached where the particles behave essentially as neutral hard spheres, independent of λ. The simulation curves in Fig. 7–10 converge therefore for large $\tilde{T}$ towards the result in eqn (1) which accurately describes the ϕ-dependence of D^r for neutral hard spheres up to the freezing transition volume fraction. With increasing ϕ, the hard-sphere plateau region is reached for smaller values of $\tilde{T}$. In the opposite limit of low $\tilde{T}$ values, the interaction of the HSY particles is dominated by the Yukawa potential part. For smaller volume fractions where $g(\sigma^+) \approx 0$ is observed, eqn (2) derived originally for low-salinity charge-stabilized particles is expected to be a decent description of D^r in the small-$\tilde{T}$ region. It is noticed that the simulation curves for λ = 3 and 8, and ϕ = 0.05 and 0.15, are indeed converging, with decreasing $\tilde{T}$, towards the result in eqn (2). Differences are visible for ϕ = 0.25 and 0.35 where eqn (2) provides only an upper bound for D^r.

We proceed with the discussion of the PA method results for D^r with full inclusion of two-sphere hydrodynamic interactions including the lubrication contribution for near-contact distances. The simulation curves for both values of λ are well reproduced by the PA approximation for ϕ = 0.05 and 0.15. This is an expected feature of this method which becomes exact at low concentrations. At higher concentrations, three-body and higher-order HIs contributions come into play which are disregarded in the simple PA treatment. As a consequence, the simulation curves for ϕ = 0.25 and 0.35 are underestimated at all values of $\tilde{T}$, *i.e.* the slowing influence of the HIs on rotational self-diffusion is overestimated. As was noticed earlier in the context of translational self-diffusion,[52] this can be attributed to the fact that the PA approximation neglects the shielding of the HIs between two particles by other particles in their vicinity. While D^r at larger ϕ is underestimated in the PA approximation, the general trends such as the relative difference between the curves for λ = 3 and λ = 8 at smaller values of the reduced temperature and the practical merging of the two curves for larger values of $\tilde{T}$ are still well predicted.

In fact, the PA method for D^r is a decent approximation up to surprisingly large volume fractions. At ϕ = 0.25, the relative difference between the PA method and simulation data for D^r depicted in Fig. 9 is less than 5% only. At the largest considered volume fraction ϕ = 0.35, the simulated D^r is underestimated by about 15% which is actually not so severe from the viewpoint of the experimental accuracy. The overall quite decent performance of the PA method with regard to short-time rotational self-diffusion should be contrasted with its performance for collective diffusion properties such as the generalized sedimentation coefficient where the concentration range of applicability is significantly narrower.[9]

We discuss next the results obtained using the revised second-order BM method. It is noticed from Fig. 7–10 that it systematically, and significantly, underestimates D^r, for all values of $\tilde{T}$ and all considered volume fractions. The relative error, $|D^r_{BM} - D^r_{sim}|/D^r_{sim}$, increases systematically with increasing ϕ, and it is more pronounced at the lower-$\tilde{T}$ side where the Yukawa repulsion is strong. In the hard-sphere-like interaction regime of large $\tilde{T}$ values, the relative error increases from about 1% at ϕ = 0.05 to 23% at ϕ = 0.35. In comparison, the relative error in the small $\tilde{T}$ region is larger, increasing from about 2% at ϕ = 0.05 to 32% at ϕ = 0.35. The most significant feature of the (revised and non-revised) BM method at higher concentrations is its weak sensitivity to changes in the range and strength of the pair potential, and to the accompanying changes in the RDF. For example, in Fig. 10 with ϕ = 0.35, the relative difference between the curves for λ = 3 and λ = 8 is four times larger for the simulation data than for the BM method curves. Incidentally, a similarly weak dependence on the shape of the pair potential and RDF has been found for the non-revised BM method result for the high-frequency viscosity of charge-stabilized suspensions.[9] In light of the controlled way in which approximations have been introduced into the revised BM method, and considering the accurate treatment of the hydrodynamic interactions, our conclusions are that the severe underestimation of D^r is basically due to the invoked mean-field type approximation of particle correlations, and to the second-order truncation in the renormalized concentration fluctuation expansion, with the latter described in part A of the ESI.†

The revised BM scheme for D^r performs somewhat better for neutral hard spheres. A direct comparison with simulation results for hard spheres (where $\lambda = \infty$ or $\tilde{T} = \infty$) is made in Fig. 11. The simulation data are well described by eqn (1) in the full liquid-phase concentration range. While the revised BM method for D^r significantly improves the original second-order BM method results for hard spheres by Treloar and Masters in the range $\phi \leq 0.4$, there is no improvement at larger volume fractions. A general observation made for the HSY systems is that the relative mean difference between revised and non-revised second-order BM results for D^r is typically 5–7% or less.

The low sensitivity of the BM method on the shape of the RDF can be related to its mean-field type structure. An important ingredient of the BM method is the effective propagator $G_{\langle \mathscr{M}_R \rangle}$ whose definition is given in part S1 of the ESI.† This propagator depends on ϕ but not on the RDF or higher-order static correlation functions. The suspension microstructure for

a given volume fraction enters into the BM approach only through renormalized concentration fluctuations included up to the second order. The truncation of the renormalized fluctuation expansion at a higher order than the second one could arguably enlarge the sensitivity of the method on the equilibrium suspension microstructure, for the price that triplet or even higher-order static distribution functions are then required as an additional input. The calculation of sufficiently precise static triplet correlation functions of concentrated suspensions is usually quite cumbersome, except in the limiting case of hard-sphere-like systems.[88]

Fig. 11 includes also the PA approximation prediction for hard spheres. The simulation data are well described by this method for $\phi \lesssim 0.25$, but D^r is increasingly underestimated at larger ϕ. This information gained from the comparison with the simulation data can be profitably used for a straightforward overall improvement of the PA method at larger concentrations for arbitrary fluid-phase HSY systems. Motivated by the large-$\tilde{T}$ plateau forms of the simulation and PA method curves in Fig. 7–10, this *ad hoc* improvement consists, for a given ϕ, of simply adding to the PA method prediction for $D^r(\tilde{T}, \lambda, \phi)$ the plateau values difference, $\Delta D^r = D^r - D^r_{PA}$, between the hard-sphere coefficient $D^r(\phi)$ accurately described by the quadratic form in eqn (1) and the corresponding PA prediction, $D^r_{PA}(\phi)$, for hard spheres. For the latter, a simple fourth-order polynomial representation of the PA curve in Fig. 11 can be used. This leads to the polynomial fitting expression

$$\Delta D^r = 0.361\phi^2 + 0.310\phi^3 + 2.264\phi^4, \qquad (22)$$

for ΔD^r valid for $\phi \leq 0.494$. We have used here that the correct first-order in concentration results for the hard-sphere $D^r(\phi)$ is reproduced by the PA method. Note that the *ad hoc* improved PA method based on eqn (22) overestimates D^r to some extent for small $\tilde{T}$ values and larger concentrations. However, this overestimation is in general less pronounced than the original underestimation of D^r at all values of $\tilde{T}$ by the non-modified PA method (*cf.* Fig. 10).

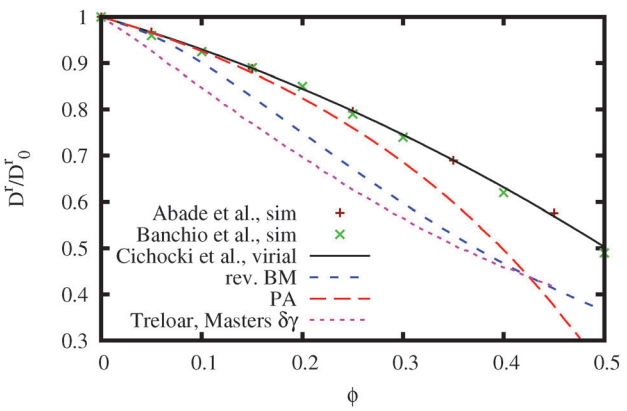

Fig. 11 Normalized rotational self-diffusion coefficient D^r/D^r_0 of neutral no-slip hard spheres as a function of ϕ. Simulation results by Abade *et al.*[33] and Banchio *et al.*[26] are compared to the second-order virial expansion result in eqn (1) by Cichocki *et al.*,[37] the original BM ($\delta\gamma$) method result by Treloar and Masters,[38] and our revised second-order BM (revised $\delta\gamma$) and PA methods predictions.

8 Summary and conclusions

We have presented a comprehensive joint theory-simulation study of short-time rotational self-diffusion in fluid-like structured suspensions of charged colloidal particles, with the direct particle interactions described by the HSY pair potential. Since this effective pair potential is generic to many different soft matter systems including ionic microgels and globular protein solutions, the presented results and discussion should be of broad interest. For the first time, a vast survey of the behavior of D^r has been made within the generic HSY model. We have quantitatively assessed the interaction parameter regions where the limiting behavior of the neutral hard-sphere and low-salinity charge-stabilized systems is reached, respectively. While these two limiting regimes have been addressed in greater detail in the past both experimentally and theoretically, very little was known about the broad transition regime of systems with intermediate salinity. This state of affairs has changed with the present paper.

A large body of high-precision simulation data for D^r was generated and compared with the results obtained using two theoretical methods. The first and more elaborate one of these theoretical methods is a revised second-order version of the original Beenakker–Mazur method which was adapted to rotational diffusion by Treloar and Masters[38] and applied by the latter two authors to no-slip hard-sphere systems. In our revised second-order BM method, various approximation steps made in the original method have been avoided, in particular regarding the treatment of the HIs which in the original BM method is rather approximate. The second semi-analytical method discussed in this work is the PA approximation with full account of two-body HI contributions including lubrication terms, but with three-body and higher-order HI contributions disregarded.

General features of D^r observed in our simulation study are its monotonic decrease with increasing $\tilde{T}$, reproduced qualitatively by both theoretical methods, and its strong sensitivity on the Yukawa potential range parameter λ for intermediate values of $\tilde{T}$. This sensitivity is well captured by the PA method, different from the revised BM method which captures this sensitivity at low concentrations only. A lower bound of D^r is provided by eqn (1) for hard spheres, reached by the simulation curves of D^r at large values of $\tilde{T}$. An upper bound is given by the scaling result in eqn (2). This upper bound is approached by the simulation curves at low values of $\tilde{T}$, provided ϕ is sufficiently small (*i.e.*, $\phi \lesssim 0.15$) and λ not very large (*i.e.*, $\lambda \lesssim 8$).

Even though HIs are accounted for to significantly higher accuracy than in the original BM and Treloar and Masters approach, the resulting improvement of D^r in our revised second-order BM method is comparatively small, amounting roughly to 5–7% for $\phi \lesssim 0.4$. A similar observation regarding the improvement by the revised BM method has been made regarding the hydrodynamic function, the short-time translational self-diffusion

coefficient, and the high-frequency viscosity of hard spheres.[30] This may be due to the interplay between mean-field and HIs approximations going into the BM method which can cause uncontrolled fortuitous cancellations or fortifications of errors.

It should be noted that the (revised) second-order BM method performs distinctly better for collective than self-diffusion properties, notably for the wavenumber dependent distinct part of the hydrodynamic function and the collective diffusion coefficient.[9] In particular concerning the distinct hydrodynamic function part, the BM method performs quite well both for hard spheres and charge-stabilized particles. In future work, it will be interesting to find out whether the overall good agreement with simulation data for the collective diffusion properties of HSY systems can be further improved by the revised method. The performance of the revised BM method regarding D^r can be possibly improved by the inclusion of third-order renormalized fluctuation contributions where, however, static three-body distribution functions are required as input to the extended method in addition to $g(r)$.

The PA method with its full account of two-body HIs contributions describes the HSY simulation data for D^r quite well for volume fractions $\phi \lesssim 0.25$. In fact, this is a rather broad concentration range considering the conceptual simplicity of this easy-to-implement method, and the fact that for HSY systems with non-small electrostatic screening lengths the freezing transition volume fraction is substantially smaller than that of neutral hard spheres. At larger concentrations, the rotational self-diffusion coefficient is significantly underestimated owing to the disregarded hydrodynamic shielding effect embodied in the neglected three-body and higher-order hydrodynamic mobility matrix contributions. Yet, general trends such as the relative difference between the D^r curves for $\lambda = 3$ and $\lambda = 8$ at smaller values of $\tilde{T}$, and the essential merging of the two curves for values $\tilde{T} \gtrsim 30$ seen in the simulations are well reproduced also at larger concentrations by the PA method. We have discussed an *ad hoc* improvement of the PA method suggested by our simulation results which is operative for larger concentrations. This improvement simply amounts to adding the polynomial expression for the hard-sphere value difference $\Delta D^r(\phi)$ in eqn (22) to the PA method prediction for D^r.

On going systematically beyond the PA approximation, three-body irreducible hydrodynamic cluster contributions to D^r could be additionally included. For low-salinity systems at lower concentrations, the leading-order far-distant three-body contributions have been accounted for already in ref. 39 in conjunction with Kirkwood's superposition approximation for the static three-body distribution function input. The long-distance three-body cluster contribution to D^r is positive valued, with the effect of bringing the value for D^r closer to the simulation data.[22,39] For larger concentrations, the calculation of sufficiently precise static triplet correlation functions is required which complicates the calculation of D^r considerably. Whether the addition of the full three-body hydrodynamic cluster contributions to the PA calculated D^r will largely and systematically improve the agreement with the simulation results for concentrated HSY systems is an open question which remains to be answered in future work.

Since the paper describes a generic study of rotational self-diffusion in fluid-phase HSY systems, we have refrained from including a comparison with specific experimental results. However, we can reasonably expect good agreement between experimental data and our high-precision simulation data for D^r, modulo unavoidable experimental scatter, for all suspensions whose static structure factor is well described using the HSY model. The microscopic details of the experimental effective pair potential, notably particle charge renormalization and specific chemical surface-charge regulation features, should play no significant role here as long as the experimental $S(q)$ is well fitted in its q-range by a HSY-based structure factor calculated using the Rogers–Young scheme. For a quick and decent estimate of D^r simply based on the experimentally determined $S(q)$, the *ad hoc* improved PA method in conjunction with the Rogers–Young fit of $S(q)$ should prove quite useful in the future.

Finally, we note that both the revised PM method and the PA approach can be rather straightforwardly extended to colloidal particles with an internal hydrodynamic structure, and hydrodynamic surface boundary conditions different from the no-slip one employed in the present work. This offers the possibility to study theoretically, *e.g.*, the rotational self-diffusion of weakly crosslinked ionic and non-ionic microgels, and of core–shell particles with a fluid-permeable soft shell.

Acknowledgements

K.M. has been supported by MNiSW grant IP2012 041572, and for the earlier part of the research work he further acknowledges support by the Foundation for Polish Science (FNP) through the TEAM/2010-6/2 project, co-financed by the EU European Regional Development Fund. M.H. acknowledges support by a fellowship within the Postdoc-Program of the German Academic Exchange Service (DAAD). G.C.A acknowledges financial support from CNPq-Brazil (Universal 480018/2013-8) and the Deutsche Forschungsgemeinschaft FOR1394, and expresses his deep gratitude to Eligiusz Wajnryb for making the HYDROMULTIPOLE simulation code available for this work. The HYDROMULTIPOLE calculations were performed at NACAD-COPPE/UFRJ in Rio de Janeiro, Brazil.

References

1 W. Van Megen, R. Ottewill, S. Owens and P. Pusey, *J. Chem. Phys.*, 1985, **82**, 508.
2 W. Van Megen and S. M. Underwood, *J. Chem. Phys.*, 1989, **91**, 552.
3 V. Degiorgio, R. Piazza and R. B. Jones, *Phys. Rev. E: Stat. Phys., Plasmas, Fluids, Relat. Interdiscip. Top.*, 1995, **52**, 2707–2717.
4 L. B. Lurio, D. Lumma, A. R. Sandy, M. A. Borthwick, P. Falus, S. G. J. Mochrie, J. F. Pelletier, M. Sutton, L. Regan, A. Malik and G. B. Stephenson, *Phys. Rev. Lett.*, 2000, **84**, 785–788.

5 G. Fritz, B. Maranzano, N. Wagner and N. Willenbacher, *J. Non-Newtonian Fluid Mech.*, 2002, **102**, 149–156.
6 D. Orsi, A. Fluerasu, A. Moussaïd, F. Zontone, L. Cristofolini and A. Madsen, *Phys. Rev. E: Stat., Nonlinear, Soft Matter Phys.*, 2012, **85**, 011402.
7 F. Westermeier, B. Fischer, W. Roseker, G. Grübel, G. Nägele and M. Heinen, *J. Chem. Phys.*, 2012, **137**, 114504.
8 A. J. C. Ladd, *J. Chem. Phys.*, 1990, **93**, 3484.
9 M. Heinen, A. Banchio and G. Nägele, *J. Chem. Phys.*, 2011, **135**, 154504.
10 A. Einstein, *Ann. Phys.*, 1906, **324**, 289–306.
11 N. Saitô, *J. Phys. Soc. Jpn.*, 1950, **5**, 4–8.
12 G. Batchelor and J. Green, *J. Fluid Mech.*, 1972, **56**, 401–427.
13 C. W. J. Beenakker and P. Mazur, *Phys. Lett. A*, 1983, **98**, 22–24.
14 C. W. J. Beenakker, *Phys. A*, 1984, **128**, 48–81.
15 C. W. J. Beenakker and P. Mazur, *Phys. A*, 1984, **126**, 349–370.
16 P. Nozieres, *Phys. A*, 1987, **147**, 219–237.
17 B. Cichocki, B. Felderhof and R. Schmitz, *Phys. A*, 1989, **154**, 233–256.
18 B. Felderhof, *Hydrodynamics of Suspensions*, in *Fundamental problems in statistical mechanics VII: proceedings of the Seventh International Summer School on Fundamental Problems in Statistical Mechanics*, Altenburg, FR Germany, 1990, June 18–30, 1989, p. 225.
19 B. Cichocki, M. L. Ekiel-Jeżewska and E. Wajnryb, *J. Chem. Phys.*, 2003, **119**, 606.
20 J. Kanetakis, A. Tölle and H. Sillescu, *Phys. Rev. E: Stat. Phys., Plasmas, Fluids, Relat. Interdiscip. Top.*, 1997, **55**, 3006.
21 G. H. Koenderink, H. Zhang, M. P. Lettinga, G. Nägele and A. P. Philipse, *Phys. Rev. E: Stat., Nonlinear, Soft Matter Phys.*, 2001, **64**, 022401.
22 G. H. Koenderink, H. Zhang, D. G. Aarts, M. P. Lettinga, A. P. Philipse and G. Nägele, *Faraday Discuss.*, 2003, **123**, 335–354.
23 G. H. Koenderink, PhD thesis, Utrecht University, 2003.
24 M. Lettinga, G. Koenderink, B. Kuipers, E. Bessels and A. Philipse, *J. Chem. Phys.*, 2004, **120**, 4517–4529.
25 D. Kleshchanok, M. Heinen, G. Nägele and P. Holmqvist, *Soft Matter*, 2012, **8**, 1584.
26 A. Banchio and G. Nägele, *J. Chem. Phys.*, 2008, **128**, 104903.
27 U. Genz and R. Klein, *Physica A*, 1991, **171**, 26–42.
28 J. Riest, T. Eckert, W. Richtering and G. Nägele, *Soft Matter*, 2015, **11**, 2821.
29 M. Wang, M. Heinen and J. F. Brady, submitted, preprint arXiv:1410.8651, 2014.
30 K. Makuch and B. Cichocki, *J. Chem. Phys.*, 2012, **137**, 184902.
31 M. Hagen, D. Frenkel and C. Lowe, *Phys. A*, 1999, **272**, 376–391.
32 R. Phillips, J. Brady and G. Bossis, *Phys. Fluids*, 1988, **31**, 3462–3472.
33 G. C. Abade, B. Cichocki, M. L. Ekiel-Jeżewska, G. Nägele and E. Wajnryb, *J. Chem. Phys.*, 2011, **134**, 4903.
34 C. Urdaneta, D. M. Jones and M. Muthukumar, *J. Chem. Phys.*, 1989, **91**, 5127–5129.
35 H. J. H. Clercx and P. Schram, *J. Chem. Phys.*, 1992, **96**, 3137.
36 H. Clercx and P. Schram, *Phys. A*, 1991, **174**, 325–354.
37 B. Cichocki, M. L. Ekiel-Jeżewska and E. Wajnryb, *J. Chem. Phys.*, 1999, **111**, 3265–3273.
38 R. Treloar and A. Masters, *Mol. Phys.*, 1989, **67**, 1273–1289.
39 H. Zhang and G. Nägele, *J. Chem. Phys.*, 2002, **117**, 5908–5920.
40 M. Watzlawek and G. Nägele, *Physica A*, 1997, **235**, 56–74.
41 G. Nägele, *Phys. Rep.*, 1996, **272**, 215–372.
42 W. Russel, W. Russel, D. Saville and W. Schowalter, *Colloidal dispersions*, Cambridge Univ Pr, 1992.
43 P. Pusey, *Liquids, Freezing and the Glass Transition*, North-Holland, Amsterdam, 1991, pp. 763–942.
44 J. K. G. Dhont, *An Introduction to Dynamics of Colloids*, Elsevier, Amsterdam, 1996.
45 S. Kim and S. Karrila, *Microhydrodynamics: Principles and Selected Applications*, Butterworth-Heinemann Boston, 1991.
46 B. Berne and R. Pecora, *Dynamic Light Scattering: with Applications to Chemistry, Biology, and Physics*, Dover Pubns, 2000.
47 R. Jones, *Phys. A*, 1988, **150**, 339–356.
48 P. Holmqvist and G. Nägele, *Phys. Rev. Lett.*, 2010, **104**, 58301.
49 M. Heinen, F. Zanini, F. Roosen-Runge, D. Fedunová, F. Zhang, M. Hennig, T. Seydel, R. Schweins, M. Sztucki, M. Antalík, F. Schreiber and G. Nägele, *Soft Matter*, 2012, **8**, 1404–1419.
50 A. Ivlev, H. Löwen, G. Morfill and C. P. Royall, *Complex Plasmas and Colloidal Dispersions: Particle-Resolved Studies of Classical Liquids and Solids*, Series in Soft Condensed Matter, World Scientific, 2012, vol. 5.
51 A. P. Philipse and A. Vrij, *J. Chem. Phys.*, 1988, **88**, 6459–6470.
52 M. Heinen, P. Holmqvist, A. Banchio and G. Nagele, *J. Appl. Crystallogr.*, 2010, **43**, 970–980.
53 M. Heinen, P. Holmqvist, A. J. Banchio and G. Nägele, *J. Chem. Phys.*, 2011, **134**, 044532.
54 M. Heinen, P. Holmqvist, A. J. Banchio and G. Nägele, *J. Chem. Phys.*, 2011, **134**, 129901.
55 K. van Gruijthuijsen, M. Obiols-Rabasa, M. Heinen, G. Nägele and A. Stradner, *Langmuir*, 2013, **29**, 11199–11207.
56 E. Trizac and Y. Levin, *Phys. Rev. E: Stat., Nonlinear, Soft Matter Phys.*, 2004, **69**, 031403.
57 L. Shapran, M. Medebach, P. Wette, T. Palberg, H. J. Schöpe, J. Horbach, T. Kreer and A. Chatterji, *Colloids Surf., A*, 2005, **270**, 220–225.
58 J. Dobnikar, R. Castañeda-Priego, H. H. von Grünberg and E. Trizac, *New J. Phys.*, 2006, **8**, 277.
59 R. Castañeda-Priego, L. F. Rojas-Ochoa, V. Lobaskin and J. C. Mixteco-Sánchez, *Phys. Rev. E: Stat., Nonlinear, Soft Matter Phys.*, 2006, **74**, 051408.
60 E. Ruiz-Reina and F. Carrique, *J. Phys. Chem. B*, 2008, **112**, 11960–11967.
61 L. F. Rojas-Ochoa, R. Castañeda-Priego, V. Lobaskin, A. Stradner, F. Scheffold and P. Schurtenberger, *Phys. Rev. Lett.*, 2008, **100**, 178304.
62 C. Labbez, B. Jönsson, M. Skarba and M. Borkovec, *Langmuir*, 2009, **25**, 7209–7213.
63 C. Calero and J. Faraudo, *J. Chem. Phys.*, 2010, **132**, 024704.

64 J. M. Falcón-González and R. Castañeda-Priego, *J. Chem. Phys.*, 2010, **133**, 216101.
65 S. A. Barr and A. Z. Panagiotopoulos, *Langmuir*, 2011, **27**, 8761–8766.
66 M. Heinen, E. Allahyarov and H. Löwen, *J. Comput. Chem.*, 2014, **35**, 275–289.
67 M. Heinen, T. Palberg and H. Löwen, *J. Chem. Phys.*, 2014, **140**, 124904.
68 H. Löwen and E. Allahyarov, *J. Phys.: Condens. Matter*, 1998, **10**, 4147–4160.
69 S. Hamaguchi, R. Farouki and D. Dubin, *Phys. Rev. E: Stat. Phys., Plasmas, Fluids, Relat. Interdiscip. Top.*, 1997, **56**, 4671.
70 M. J. Stevens and M. O. Robbins, *J. Chem. Phys.*, 1993, **98**, 2319–2324.
71 A.-P. Hynninen and M. Dijkstra, *Phys. Rev. E: Stat., Nonlinear, Soft Matter Phys.*, 2003, **68**, 021407.
72 J. Gapinski, G. Nägele and A. Patkowski, *J. Chem. Phys.*, 2012, **136**, 024507.
73 J. Gapinski, G. Nägele and A. Patkowski, *J. Chem. Phys.*, 2014, **141**, 124505.
74 J.-P. Hansen and L. Verlet, *Phys. Rev.*, 1969, **184**, 151.
75 K. Kremer, M. O. Robbins and G. S. Grest, *Phys. Rev. Lett.*, 1986, **57**, 2694–2697.
76 D. C. Wang and A. P. Gast, *J. Phys.: Condens. Matter*, 1999, **11**, 10133.
77 J.-P. Hansen and I. R. McDonald, *Theory of Simple Liquids*, Academic Press, London, 3rd edn, 1986.
78 F. J. Rogers and D. A. Young, *Phys. Rev. A: At., Mol., Opt. Phys.*, 1984, **30**, 999–1007.
79 J. Gapinski, A. Wilk, A. Patkowski, W. Häuler, A. J. Banchio, R. Pecora and G. Nägele, *J. Chem. Phys.*, 2005, **123**, 054708.
80 J. Gapinski, A. Patkowski, A. Banchio, J. Buitenhuis, P. Holmqvist, M. Lettinga, G. Meier and G. Nägele, *J. Chem. Phys.*, 2009, **130**, 084503.
81 M. Robles, M. López de Haro and A. Sántos, *J. Chem. Phys.*, 2014, **140**, 136101.
82 M. D. Carbajal-Tinoco, *J. Chem. Phys.*, 2008, **128**, 184507.
83 B. Cichocki, B. Felderhof, K. Hinsen, E. Wajnryb and J. Bawzdziewicz, *J. Chem. Phys.*, 1994, **100**, 3780.
84 B. Cichocki, B. U. Felderhof and R. Schmitz, *PhysicoChem. Hydrodyn.*, 1988, **10**, 383–403.
85 B. Cichocki, R. B. Jones, R. Kutteh and E. Wajnryb, *J. Chem. Phys.*, 2000, **112**, 2548.
86 R. B. Jones and R. Schmitz, *Phys. A*, 1988, **149**, 373–394.
87 D. Jeffrey and Y. Onishi, *J. Fluid Mech.*, 1984, **139**, 261–290.
88 J. Brader, *J. Chem. Phys.*, 2008, **128**, 104503.

